Princeton Plasma Physics Laboratory

PPPL- 4970

PPPL- 4970

Development of an Electrostatic Detectoor for Tungsten Dust

Kenneth C. Hammond and Charles Skinner

DECEMBER, 2013

PPPL PRINCETON PLASMA PHYSICS LABORATORY

Prepared for the U.S. Department of Energy under Contract DE-AC02-09CH11466.

Princeton Plasma Physics Laboratory
Report Disclaimers

Full Legal Disclaimer

Trademark Disclaimer

PPPL Report Availability

Princeton Plasma Physics Laboratory:

http://www.pppl.gov/techreports.cfm

Office of Scientific and Technical Information (OSTI):

http://www.osti.gov/bridge

Related Links:

U.S. Department of Energy

Office of Scientific and Technical Information

Fusion Links

Development of an Electrostatic Detector for Tungsten Dust

Kenneth C. Hammond
Harvard University
Cambridge Mass

Charles Skinner
Princeton Plasma Physics Lab
P O Box 451, Princeton NJ 08543

Abstract

Large inventories of dust are expected in next-step fusion reactors such as ITER, and dust detection devices will be necessary to manage the associated hazards. Electrostatic dust detectors have been successfully used to detect graphite dust on NSTX and Tore Supra. These detectors consist of interlocking copper conducting combs on a circuit board that are biased to 50V. Impinging dust particles cause temporary short circuits that produce measurable electronic signals. We have constructed a more rugged version of this device for the detection of tungsten particles in which the conducting combs are themselves made of tungsten wire, and the interwire spacing and bias voltage are an order of magnitude higher. Initial tests have shown a good response to incident tungsten particles and the tungsten wires were far more durable than the copper traces used previously. We will present data on some electrostatic effects that became apparent at the higher voltages used, and initial results on the detector sensitivity.

I. Introduction

Dust formation, caused primarily by plasma-wall erosion, is a common occurrence in magnetic fusion devices [1]. Having only a minimal presence in current devices, dust has as yet been of little concern. The larger amounts of dust expected in next-step reactors such as ITER [1], however, may cause plasma contamination [2] and could pose public safety risks if accidentally released into the environment [1]. Consequently, ITER project requirements mandate that reactor dust levels be limited to 1000 kg [3] and that they be measured with 20% relative and 50% absolute accuracy [4].

An *in situ* diagnostic for measuring dust levels on surfaces will be necessary to meet those requirements. One such device currently in development is the electrostatic dust detector [5]–[9]. In essence, the detector consists of a pair of interlocking conducting combs with a voltage bias between them. Incident particles cause a temporary short circuit that can be registered by signal detection equipment. Recent versions of this design have been successfully tested on NSTX [9] and Tore Supra [10]. Both detectors were constructed by printing copper traces on 50.8 mm square circuit boards with a 25 μm trace spacing and 50 V bias voltage. The results from both tokamaks showed that plasma disruptions were a major source of dust [9], [10].

These detectors need further development to be suitable for ITER. ITER will contain tungsten plasma-facing components, and previous work showed that the copper traces could be damaged by a short circuit with tungsten dust. An electrostatic dust detector for ITER thus must be constructed with more rugged materials. In this paper, we describe initial tests of two detectors whose combs are made of tungsten wire. First, we will describe the designs of the detectors and outline their potential advantages and disadvantages. We will then present the

experimental setup, data acquisition system, and results. Finally, conclusions will be presented in addition to plans for future design improvements.

II. Detector Designs

a. Rectangular detector

The first detector (Fig. 1) used 0.25 mm diameter tungsten wire supported by a rectangular 25 mm x 44 mm block of boron nitride (BN). Twenty-four straight 0.18 mm deep, 0.30 mm wide grooves spaced 0.20 mm apart were machined across the face. Segments of straight tungsten wire 44 mm long were placed in the grooves, and arranged as shown in Figs. 2–4. The wires were held in place by polyether ether ketone (PEEK) clamps. Alternate wires extended over the left or right side of the block and were clamped between layers of copper foil. In this way each set of alternating wires became interlinked as a comb and could be held at a different electric potential from the other set. Copper wires were attached to each comb to connect the detector to the external power supply and detection equipment.

b. Cylindrical detector

Smaller-scale wires and wire spacing are advantageous as they produce a given electric field at lower voltages. Previous detectors with the lowest spaced copper traces were the most sensitive [6]. However, the mechanical stiffness of fine tungsten wire made it difficult to wrap wire continuously on a rectangular form. A cylindrical form (without sharp corners), adopted for 0.13 mm diameter tungsten wire, was built on a 25 mm diameter Delrin cylinder (Fig. 5). Two grooves, with depth, width, and spacing equal to the wire diameter, were machined into the

surface to form a double helix with twenty-five turns (Fig. 6). Two wires were attached to the form, which was then held in a lathe chuck and rotated by hand to wrap the wires. The wires were held in constant tension and guided into alternating grooves in the double helix. In this way, the wires effectively formed a comb and were not in contact with one another. Copper wires were attached to the end of each tungsten wire to connect the detector to the detection circuitry.

c. Comparison with previous designs

Both detector designs could be assembled in-house and, if damaged, could be quickly disassembled and repaired (especially the rectangular design). This stands in contrast to the copper detectors, for which in-lab repairs were impossible and the detector needed to be replaced in the event of permanent damage. The present design was also generally more resistant to wear and tear than the copper design, whose micron-scale copper traces could be damaged by mechanical abrasion.

On the other hand, the spacing between the tungsten wires was 5x–20x greater than that of the copper detectors. It had been found in studies with the copper detectors that finer spacing led to greater sensitivity to dust and more accurate measurements [5]–[8]. However, we expect that the large amounts of dust predicted in ITER (orders of magnitude greater than the concentrations in current tokamaks) will not require the ultra-high sensitivity of the copper detectors.

Another major departure from older models was in the voltage bias applied to the detectors. Previous work with the copper detectors [5] showed that the optimal bias voltage was 50 V for a trace spacing of 0.025 mm, corresponding to an electric about 65% of the breakdown field in air (which is approximately 3.3 kV/mm [11]). To produce the same electric field on the

more coarsely spaced tungsten comb, a higher voltage was required (350 V and 800 V for tungsten wire spacings of 0.13 mm and 0.25 mm, respectively).

III. Laboratory Setup

The experimental setup (Fig. 7) was similar to that described in [8]. Testing took place inside a chamber consisting of a 100 mm diameter pipe with 150 mm Conflat flanges at the top and bottom. The detector was mounted on the bottom flange. Dust was loaded into a square supply tray with a 3.8 mm square layer of wire mesh with 104 μm square apertures at the bottom. The loaded tray was placed in a holder suspended below the top flange, which was then affixed to the top of the test chamber. Dust was released from the tray by applying a mechanical vibrator to the top flange. Between dust deposition trials, residual dust was blown off the detector area with a can of compressed gas.

The tungsten dust used in this experiment was supplied by Alldyne Powder Technologies, 7300 Highway 20 W, Huntsville, AL 35806. To measure the size of the dust particles, dust was shaken onto a microscope slide from the supply tray and different regions of the slide were photographed at 4x magnification (Fig. 8). Some dust particles appeared to form clumps (Fig. 9). The dust images were analyzed with ImageJ software [12], which determined the average projected area of the particles to be 575 μm^2 with a standard deviation of 965 μm^2. Individual particles were observed to be of ~ 10 μm scale. The median diameter is calculated to be 16.1 μm but this includes the clumps that were counted as single particles in the ImageJ analysis.

To determine the amount of mass released from the supply tray during testing, the tray was weighed before and after each trial with a Sartorius ME5-F microbalance with 1 μg resolution, 5 g capacity, and a 51 mm diameter pan that was recalibrated once to twice a day to compensate for changes in room temperature. To check the amount of mass incident on the detector, an aluminum foil collecting tray was placed over the detector area. The mass gain of the collecting tray was found to be 85–95% of the mass lost by the dust supply tray. The percentage of dust incident on the cylindrical detector is expected to be as high or higher since its area is larger.

During the trials, the detector was biased to a voltage between 100 and 800 V by either a Bertran Associates, Inc. Model 315 DC power supply with 5000 V, 5 mA capacity or a Kepco ATE 325-0.8M DC supply with 350 V, 0.8 A capacity (Fig. 10). In some trials, a 0.01 μF capacitor was connected in parallel with the voltage source to provide an extra source of current at the beginning of a short circuit in the detector. The pulse from a short circuit is attenuated by a factor of 116 by a 4.3 Ω / 500 Ω potential divider and filtered by a 1.3Hz high-pass filter in parallel to produce a waveform suitable for the detection electronics [5]. The signal was displayed on a Tektronix TDS5054B-NV oscilloscope and input to an Ortec 550 single-channel analyzer (SCA). The SCA generated a pulse that was counted by an Ortec 775 counter (range 0–999 999) every time the input signal to the SCA fell below a specified level (0.4 V for the results presented in this paper). The SCA response time was listed by the manufacturer as 100 ns plus the output pulse width of 500 ns.

IV. Results

When dust was distributed onto a non-energized detector, it would form a pile on the detector grid as expected. However, if the detector was energized to a sufficiently high voltage, most of the dust would be found just outside the detector area with the grid essentially clear of dust. This effect became noticeable at voltages in the mid 100s of volts; above 300 V almost no dust would remain on the grid (Figs. 11–15). At intermediate voltages in the range from 150 V to 300 V, most of the dust that remained in the detector area after deposition was positioned adjacent to wires that had been energized during testing (Figs. 12, 13). Dust also adhered to the vertical PEEK walls of the rectangular detector. This effect was not seen below 100 V, and was not apparent earlier detectors that were operated at 50 V. In one trial, dust was deposited onto an energized detector grid with wire diameter and spacing of 0.5 mm that was covered with a layer of insulating Kapton tape. The dust particles in this case distributed at locations on the tape surface above energized wires (Fig. 16). In contrast, the grid area was mostly dust-free after the trials with the grid exposed.

Tests at 800V on the rectangular detector yielded pulses that were on the order of 100 μs in length, beginning with a rapid spike and ending with a rapid drop followed by exponential decay (Fig. 17). The 0.01 μF capacitor enhanced the initial spike as may be seen by comparing Fig. 17 (with capacitor) with Fig. 18 (without). The decay time after the restoration of the open circuit matched the characteristic RC time constant of the loop with the 0.1 μF capacitor (Fig. 10). At 800 V it was common for envelope pulses to contain sets of rapid (~ 3 MHz) oscillations such as the one shown in fig. 15 at 1570 μs. At lower voltages (<400 V), however, the envelope

signals were much narrower – on the order of 1 μs (Fig. 19) rather than 100 μs as with the 800 V signal in Fig. 17.

It is important to note that counts were not triggered continuously during dust deposition. Rather, they came in intermittent bursts. The frequency of these bursts varied and was generally much greater for the cylindrical detector than the rectangular detector: gaps between bursts in the former were rarely longer than 10 s, whereas the latter routinely exhibited gaps of 30 s or more. Many tests with the rectangular detector recorded no counts at all (in one case, more than 14 mg of dust had been administered to the detector with no response), and only the cylindrical detector exhibited periods of continuous count recording.

Occasionally, stains would appear on the detector during testing (Fig. 20). Stains on the soft BN surface of the rectangular detector were usually easy to remove with sand paper. On some occasions stained divots would form beneath a PEEK clamp, requiring a disassembly of the detector to sand off the BN surface as well as the PEEK. The stains on the PEEK, which formed in divots, required far more sanding to remove than those in the BN. Overall, of sixty-nine tests with the rectangular detector in which shorting occurred, three left stains that resulted in continuity between opposing combs.

Between tests with the cylindrical detector, neither the compressed gas can nor an alcohol-soaked wipe could remove all of the dust from the grid area. Most of this adherent dust made contact with wires. During one of the tests, counts were continuously recorded well after the period of dust deposition and did not stop until the power supply was shut off. In this case, the top flange was removed from the test chamber after dust deposition but while counts were still being registered, and repeated flashes of light were seen from a single location on the grid.

The last three tests with the cylindrical detector were conducted with 0.56 μF in parallel with the power supply (rather than the 0.01 μF shown in Fig. 10). During the last test one of the wires broke apart, and a divot was observed in the detector where the break occurred.

We present two plots of counts versus mass of dust released from the tray in the test chamber. Fig. 21 presents data from tests with the rectangular detector energized to 800 V; Fig. 22 presents data from tests with the cylindrical detector energized to 350 V. Tests that resulted in permanent shorts or counts occurring after the deposition period were not included in these plots.

V. Discussion

The tendency of the dust to deflect from the detector grid was not observed in previous detectors because they were biased to voltages below the point at which this effect became apparent. Our proposed explanation for this effect is as follows. When neutral tungsten dust falls toward the detector area with some wires at a positive high voltage and other wires grounded, the free electrons in the conducting particles arrange themselves so that the wire-facing side of the particle attains a negative charge and the opposite side attains a positive charge [13]. Because the negatively charged region is marginally closer to the positively charged wires, the dust particle experiences a net attractive force toward the charged wires. Dust with a net negative charge would also experience attraction to the positively charged wires. This initial attraction would explain the behavior of the dust when it was prevented from making direct contact with the wires by Kapton tape (Fig. 19). Upon contact with the charged wires, the dust itself obtains a positive static charge and is repelled from the high-voltage wires, possibly with sufficient velocity to be ejected from the detector area altogether. As for why this effect was diminished at lower

voltages, we speculate that oxide coatings on the dust and/or wires inhibited the transfer of charge on contact between particles and wires. At higher voltages (beginning in the mid 100s of volts), the voltage may have been sufficient to break down these coatings and allow the dust particles to become charged. In support of this hypothesis, we note that most of the dust that remained in the detector area after a deposition onto wires at an intermediate voltage (100–300 V) appeared to remain attracted to the energized wires (i.e. dust that was unable to obtain charge from the energized wires was attracted to them; see Fig. 12).

A plot of counts vs. incident dust mass is shown in Fig. 21 for the rectangular detector and Fig. 22 for the cylindrical detector. A comparison of the results indicates that the latter was more sensitive to impinging dust in terms of counts per unit mass. This is supported by the observation that periods of SCA inactivity during dust deposition were longer for the rectangular detector. In addition, the inter-wire electric field on the cylindrical detector was 88% of that of the rectangular detector at only 44% of the wire voltage. Thus it appears that, for a given field strength, detectors with lower voltage bias will be more sensitive than those with higher voltage.

Despite the apparent decrease in sensitivity brought about by the electrostatic repulsion effect, the effect is still potentially useful as a self-cleaning mechanism. Small amounts of residual dust were observed on previous detectors, and various systems were conceived for removing this dust from the surface during operation [14]–[16]. If the detector exhibited this self-cleaning mechanism without excessively inhibiting sensitivity, the need for such auxiliary systems would be eliminated. The deflection effect would also likely serve to prevent instances – as observed in the cylindrical detector – of a single particle or group of particles remaining on the grid and causing multiple arcs, likely a source of inaccuracy in the counting system.

Further inhibiting counting accuracy is the tendency of the detectors to produce short-circuit responses only intermittently during dust depositions. We have observed long stretches in which impinging dust goes unnoticed, especially with the rectangular detector, suggesting that the counts recorded may not provide a reliable measurement of the incident dust. A successful detector needs to be sensitive enough to produce short-circuit signals whenever dust is impinging on its surface, or at least when dust is depositing quickly enough to be considered significant.

Another inhibition to counting accuracy might be the rapid ~ 3 MHz oscillations that appeared in the wider (100 μs scale) envelope signals generated by the detector. While the source of these oscillations has not been identified, they did not appear to correlate with the amount of dust hitting the detector (they would appear at random locations in the waveform, even in signals of arcs from open-air breakdown). Nevertheless, they can trigger the SCA, resulting in an unpredictable number of counts for each pulse from the detector and making it difficult to relate counts to total incident mass. However, under conditions in which the signal duration is of 1 μs scale and thus not much wider than the SCA pulse itself, the SCA would not be able to generate more than one (or possibly two) 500 ns pulses per short. (The signal duration varied from ~ 100 μs at 800 V bias to ~ 1 μs at voltages less than 400 V for reasons that have yet to be determined.) This suggests that energizing the grid to voltages that generate dust signals of 1 μs or less would be conducive to SCA counts that more accurately represent the amount of dust that falls on the detector grid.

The observed difficulty in removing dust from the grid of the cylindrical detector may be due to the particles becoming lodged in the Delrin material after heating from arc events. Trapped dust is likely to lead to the repeated arcing effect discussed above. Future cylindrical detectors should be made of a different material, possibly a harder BN compound.

Throughout our testing, we struggled to establish a meaningful relationship between the number of counts and the mass of dust administered to the detector for the reasons outlined above. Our best results so far, displayed in Fig. 22, are from depositions onto the cylindrical detector at 350 V. These conditions provided good sensitivity and resulted in pulses of ~ 1 μs length that prevented extraneous SCA counts. The large spread in the results, however, indicates that improvement is still needed. Although sensitivity was the best we had obtained so far, there were still periods during dust deposition when no counts were registered. Some of the isolated periods of rapid counts that were observed could have arisen from repeated arcing. Furthermore, the detector eventually broke during a deposition period, emphasizing the need for further design improvements.

VII. Conclusion and future work

Despite the multiple challenges presented by the tungsten detector, our tests have clearly indicated that electrostatic detectors have the potential to detect tungsten dust. Although we observed one broken wire, the tungsten wires overall were far more durable than the copper traces used in previous detectors. Dust was ejected from the detector grid if it was energized to sufficiently high voltages (>150V). Finally, the number of counts registered for the cylindrical detector operated at 350 V increased with the mass of the impinging dust in an approximately linear relation, albeit with some scatter due to the factors discussed above.

The tungsten detector requires more work, however, to be viable as an ITER device. For one, more diagnostic work is needed to further characterize the detector's behavior. High-speed camera observations to track the behavior of the dust at the detector surface would reveal more

about the dust's tendency to deflect at high voltages. Exposing falling dust to a separate electric field could indicate if the falling dust was charged. Since dust that falls through the ITER plasma is likely to be charged itself, it would be germane to conduct tests using dust that has been deliberately charged before application. It would also be useful to determine the dependence of SCA counts on the rate at which dust falls on the detector.

Once conditions are found that facilitate a more reproducible relationship between dust mass and counts, it will be necessary to test the detector under vacuum conditions. This means that a material other than Delrin must be used for the cylindrical detector due to its outgassing properties (although Delrin had already shown itself to be subpar due to its apparent tendency to lodge dust particles). Another issue that will arise when testing in ITER conditions will be the oxide coatings that we have presumed to exist on the dust and the wires during our non-vacuum tests but will be absent on dust generated in ITER. Oxide coatings have played a role in our proposed explanation for the dust deflection effect, so it is desirable to see how this effect changes in absence of the coatings. Tungsten dust in ITER is also not expected to exhibit clumping (as in Fig. 9), and tests with more ITER-like particles are needed.

VII. Acknowledgements

The authors would like to thank T. Holoman, M. Karlik, D. Labrie, T. Provost, H. Schneider, G. Smalley, and J. Trafalski for their invaluable assistance and expertise. This work was supported by a grant from the Department of Energy – SULI Program through contract no. DE-AC02-09CH11466.

References

[1] G. Federici, C.H. Skinner, J.N. Brooks, J.P. Coad, C. Grisolia, A.A. Haasz, A. Hassanein, V. Philipps, C.S. Pitcher, J. Roth, W.R. Wampler, and D.G. Whyte, "Plasma-material interactions in current tokamaks and their implications for next-step fusion reactors," *Nuclear Fusion*, vol. 41, no. 12, p. 1967, Dec. 2001.

[2] S.I. Krasheninnikov, Y. Tomita, R.D. Smirnov, and R.K. Janev, "On dust dynamics in tokamak edge plasmas," *Physics of Plasmas*, vol. 11, no. 6, pp. 3141-3150, June 2004.

[3] S. Rosanvallon, C. Grisolia, P. Andrew, S. Ciattaglia, P. Delaporte, D. Douai, D. Garnier, E. Gauthier, W. Gulden, S.H. Hong, S. Pitcher, L. Rodriguez, N. Taylor, A. Tesini, S. Vartanian, A. Vatry, and M. Wykes, "Dust limit management strategy in tokamaks," *Journal of Nuclear Materials*, vol. 390-391, pp. 57-60, 2009.

[4] ITER_Diagnostic_Project_Requirements_(PR)_27ZRW8_v4_0

[5] A. Bader, C.H. Skinner, A.L. Roquemore, and S. Langish, "Development of an electrostatic dust detector for use in a tokamak reactor," *Review of Scientific Instruments*, vol. 75, no. 2, pp. 370-375, Feb. 2004.

[6] C. Voinier, C.H. Skinner, and A.L. Roquemore, "Electrostatic dust detection on remote surfaces," *Journal of Nuclear Materials*, vol. 346, no. 2-3, pp. 266-271, Nov. 2005.

[7] C.H. Skinner, R. Hensley, and A.L. Roquemore, "Large aperture electrostatic dust detector," *Journal of Nuclear Materials*, vol. 376, no. 1, pp. 29-32, May 2008.

[8] D.P. Boyle, C.H. Skinner, and A.L. Roquemore, "Electrostatic dust detector for fusion devices with improved sensitivity," *Journal of Nuclear Materials*, vol. 390-391, pp. 1086-1089, June 2009.

[9] C.H. Skinner, B.Rais, A.L. Roquemore, H.W. Kugel, R. Marsala, and T. Provost, "First real-time detection of surface dust in a tokamak," *Review of Scientific Instruments*, vol. 81, p. 10E102, Oct. 2010.

[10] H. Roche et al., submitted to Physica Scripta, 2011.

[11] A.M. Howatson, "Breakdown," *An Introduction to Gas Discharges*, Pergamon Press, 1965, p. 67.

[12] See http://rsbweb.nih.gov/ij/ for ImageJ information (August 2011).

[13] D.W. Griffiths, "Electrostatics," *Introduction to Electrodynamics*, 3rd ed. Upper Saddle River, NJ: Prentice-Hall, 1999, p. 98.

[14] A. Campos and C.H. Skinner, "Advances in Dust Detection and Removal for Tokamaks," *U.S. D.O.E. Journal of Undergraduate Research,* vol. 9, pp. 30-35, 2008. http://science.energy.gov/wdts/opportunities-for-undergraduate-students/journal-of-undergraduate-research/volume-9

[15] B. Rais, C.H. Skinner, and A.L. Roquemore, "He puff system for dust detector upgrade," *Review of Scientific Instruments*, vol. 82, March 2011, p. 036102.

[16] F.Q.L. Friesen, B. John, C.H. Skinner, A.L. Roquemore, and C.I. Calle, "Evaluation of an electrostatic dust removal system with potential application in next-step fusion devices," *Review of Scientific Instruments*, vol. 82, May 2011, p. 053502.

Figure Captions

Fig. 1: Rectangular detector assembly on flange: (a) tungsten wire, (b) PEEK clamp, (c) BN block, (d) wire connecting to power supply, (e) wire connecting to detection circuitry, (f) copper foil linking overlapping wires, (g) feed-through.

Fig. 2: Diagram of wire arrangement on rectangular detector: (a) BN block, (b) copper foil contact, (c) wires linking to power supply and detection circuitry, (d) holes for attaching PEEK clamp, (e) holes for attaching detector to studs on flange, (f) location of cross section depicted in Fig. 3.

Fig. 3: Cross section of wires between copper foil and PEEK clamps: (a) wires, (b) copper foil layers, (c) stainless steel bars, (d) PEEK clamp. The layers are clamped together by nuts and bolts through the holes shown in Fig. 2.

Fig. 4: Cross section of wires in grooves on rectangular detector.

Fig. 5: Cylindrical detector assembly on flange: (a) two 0.13mm tungsten wires arranged in a double helix, (b) Delrin cylinder, (c) screw securing tungsten wire to external connector, (d) wire connecting to power supply, (e) wire connecting to detection circuitry, (f) feed-through.

Fig. 6: Cross section of wires in grooves on cylindrical detector.

Fig. 7: Laboratory setup.

Fig. 8: Microscope image (4x magnification) of tungsten particles used in this experiment. The width of the image is approximately 2.67mm.

Fig. 9: Microscope image at 40x magnification showing examples of clumping. Image is approximately 270μm wide.

Fig. 10: Schematic of the circuit used for the tests. The 500Ω and 4.3Ω resistors adjust the magnitude of the signal received by the oscilloscope and SCA. The 62Ω resistor was part of a low-pass filter used in previous experiments.

Fig. 11: Rectangular detector after dust deposition while energized to 150V.

Fig. 12: Rectangular detector after dust deposition while energized to 250V.

Fig. 13: Rectangular detector after dust deposition while energized to 250V.

Fig. 14: Rectangular detector after deposition while energized to 300V.

Fig. 15: Dust deposition on a rectangular detector whose wires were covered with insulating tape. Dust has lined up along the wires that were at high voltage. (Note: this particular detector

had wire diameters and spacing of 0.50 mm, twice that of the rectangular detector referred to by default in this paper.)

Fig. 16: Cylindrical detector after deposition while energized to 350V.

Fig. 17: Signal from the rectangular detector during a short circuit at 800V (top) and the response pulses from the SCA (bottom; offset and scaled for clarity). A 0.01 μF capacitor was in parallel with the power supply. Note that in absence of the rapid oscillations, the signal would have generated only one SCA pulse (the one at ~ 1600 μs). Time is measured relative to the triggering of the oscilloscope.

Fig. 18: Typical signal from the rectangular detector biased to 800 V with no capacitance in parallel with the power supply.

Fig. 19: Signal from cylindrical detector during a short circuit at 350 V (top) and response pulses from the SCA (bottom; offset and scaled for clarity). A 0.01 μF capacitor was in parallel with the power supply. Time is measured relative to the triggering of the oscilloscope.

Fig. 20: Example of a conducting stain found on the rectangular detector, underneath a PEEK clamp.

Fig. 21: Scatter plot of counts recorded for given amounts of dust released from the supply tray for the rectangular detector energized to 800V.

Fig. 22: Scatter plot of counts recorded for mass released from the supply tray for the cylindrical detector energized to 350V.

Figures

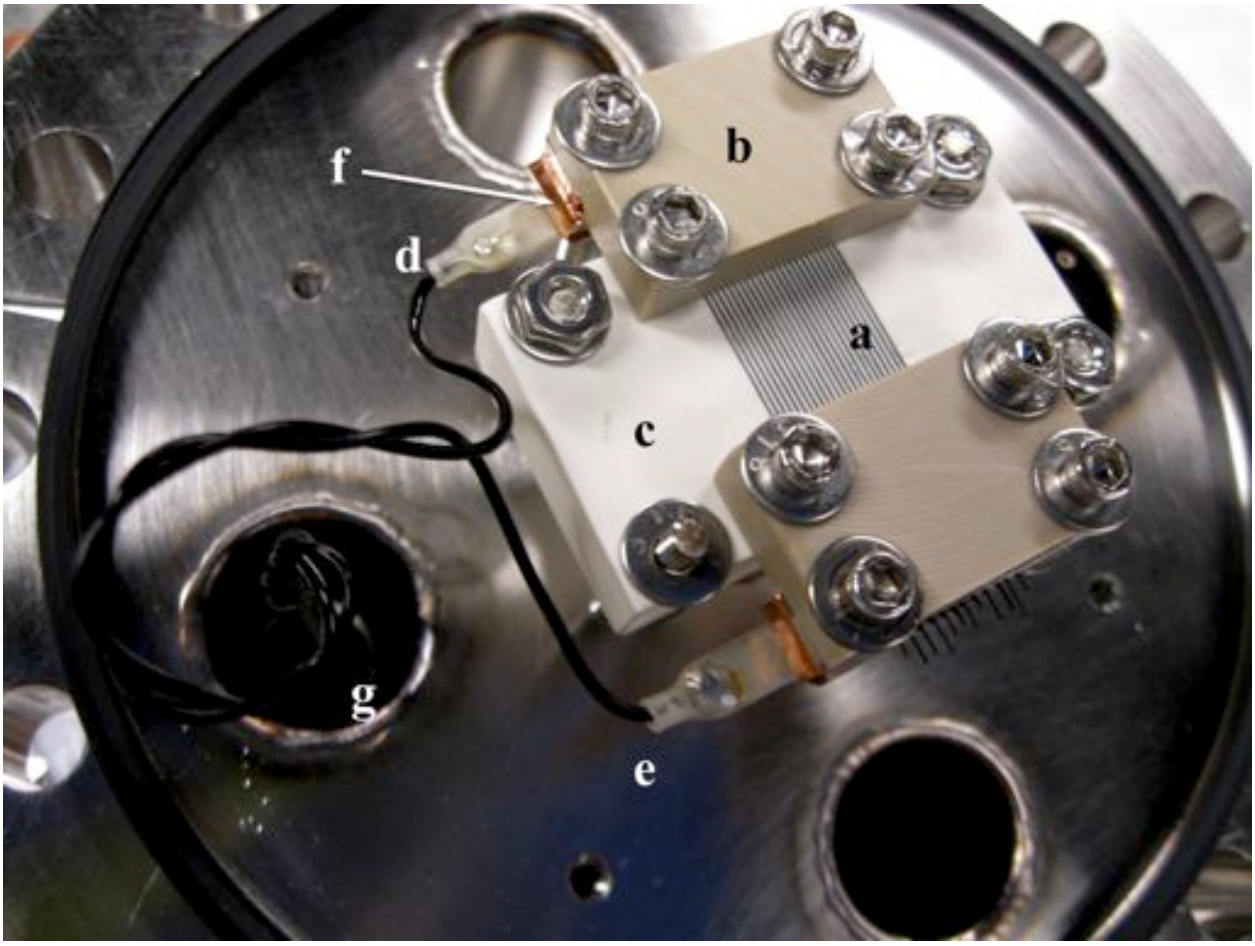

Fig. 1: Rectangular detector assembly on flange: (a) tungsten wire, (b) PEEK clamp, (c) BN block, (d) wire connecting to power supply, (e) wire connecting to detection circuitry, (f) copper foil linking overlapping wires, (g) feed-through.

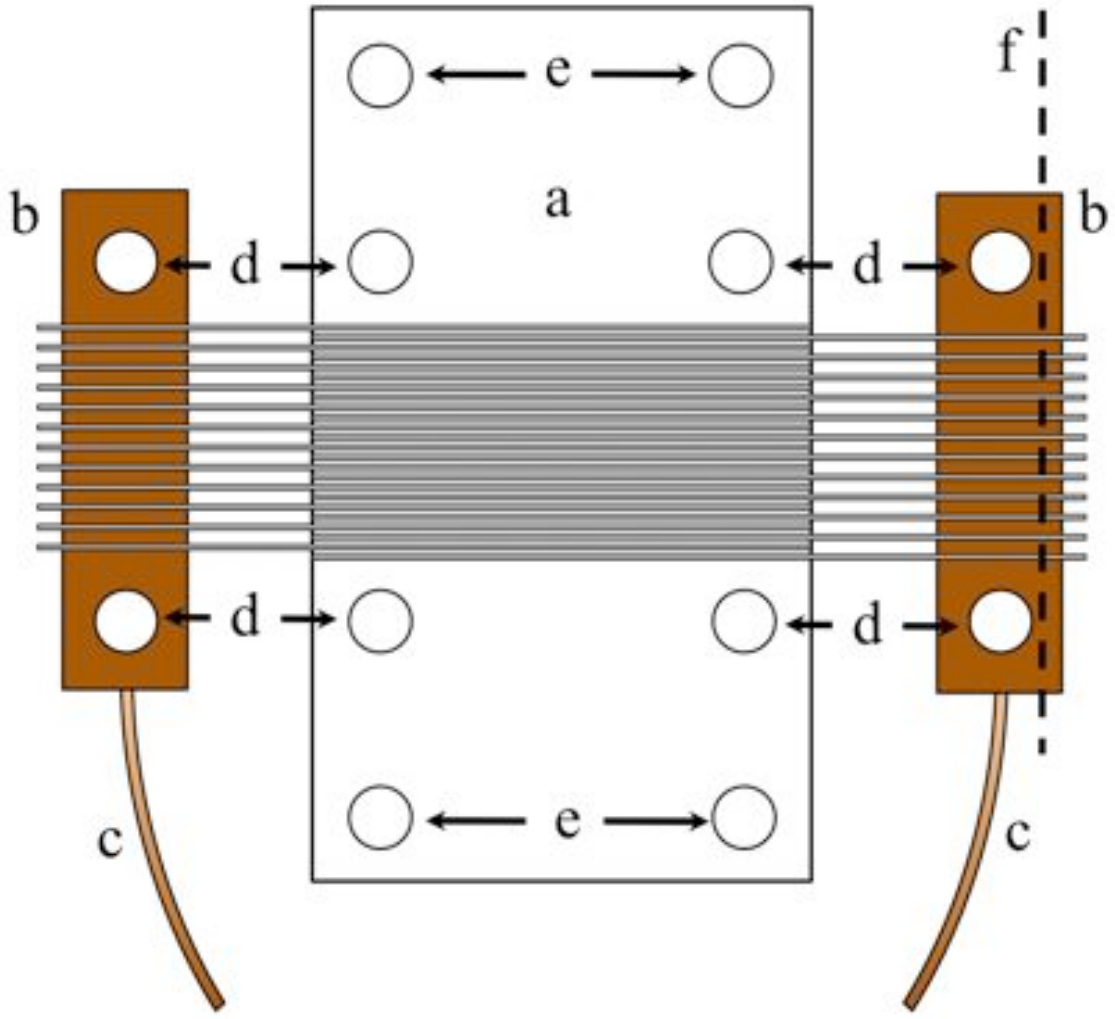

Fig. 2: Diagram of wire arrangement on rectangular detector: (a) BN block, (b) copper foil contact, (c) wires linking to power supply and detection circuitry, (d) holes for attaching PEEK clamp, (e) holes for attaching detector to studs on flange, (f) location of cross section depicted in Fig. 3.

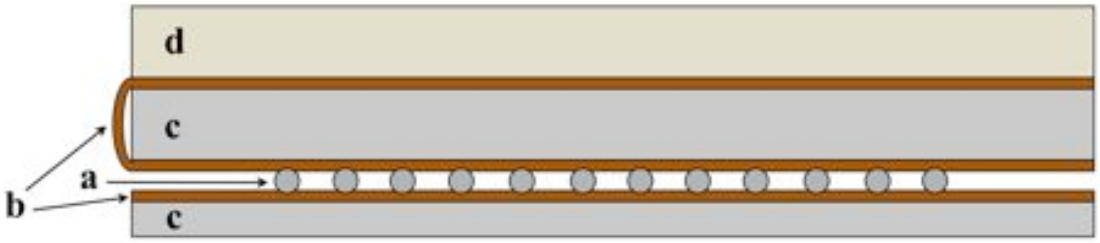

Fig. 3: Cross section of wires between copper foil and PEEK clamps: (a) wires, (b) copper foil layers, (c) stainless steel bars, (d) PEEK clamp. The layers are clamped together by nuts and bolts through the holes shown in Fig. 2.

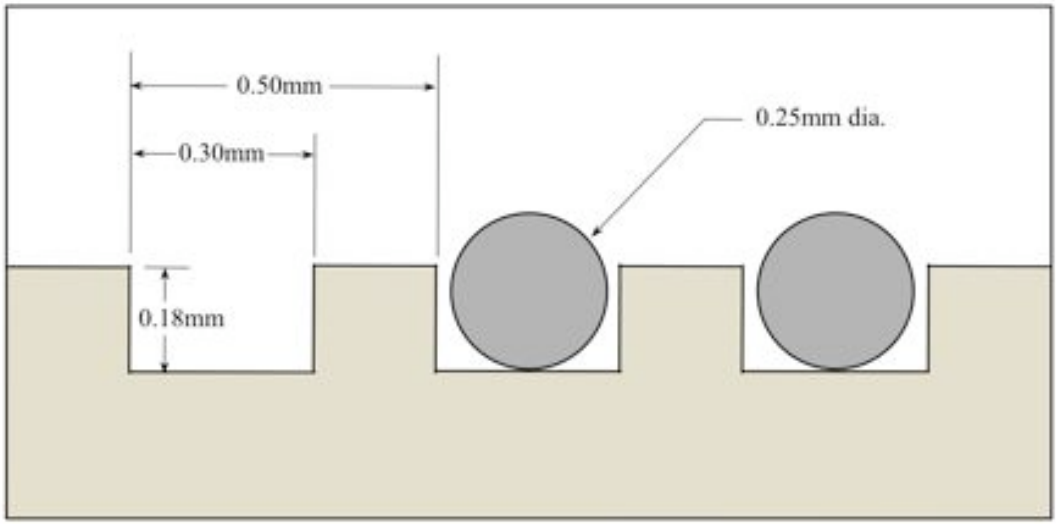

Fig. 4: Cross section of wires in grooves on rectangular detector.

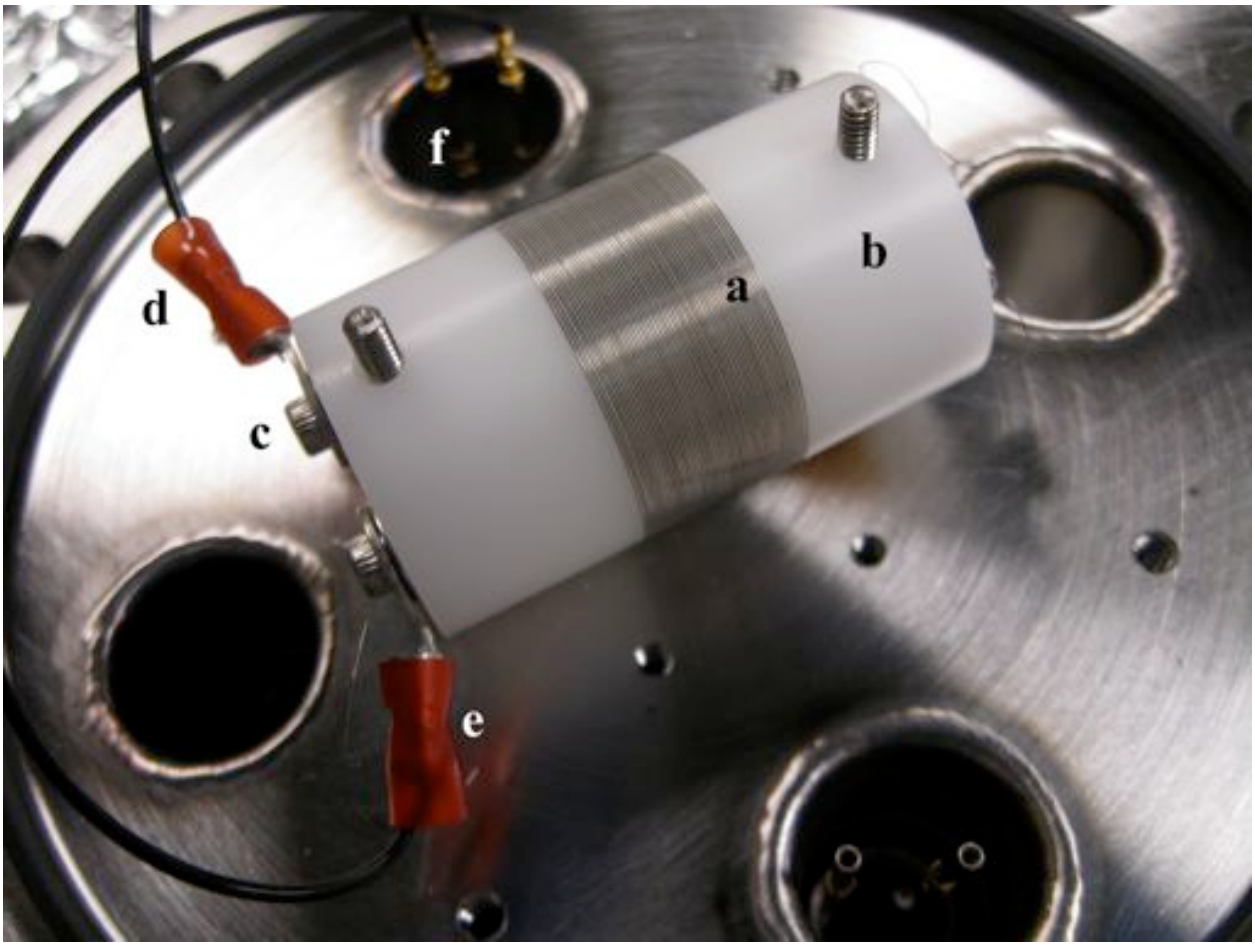

Fig. 5: Cylindrical detector assembly on flange: (a) two 0.13mm tungsten wires arranged in a double helix, (b) Delrin cylinder, (c) screw securing tungsten wire to external connector, (d) wire connecting to power supply, (e) wire connecting to detection circuitry, (f) feed-through.

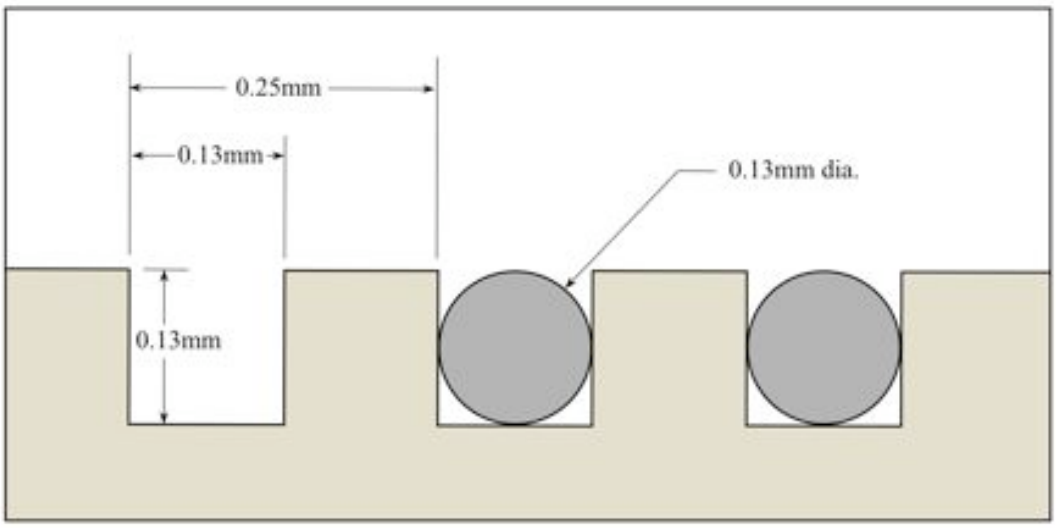

Fig. 6: Cross section of wires in grooves on cylindrical detector.

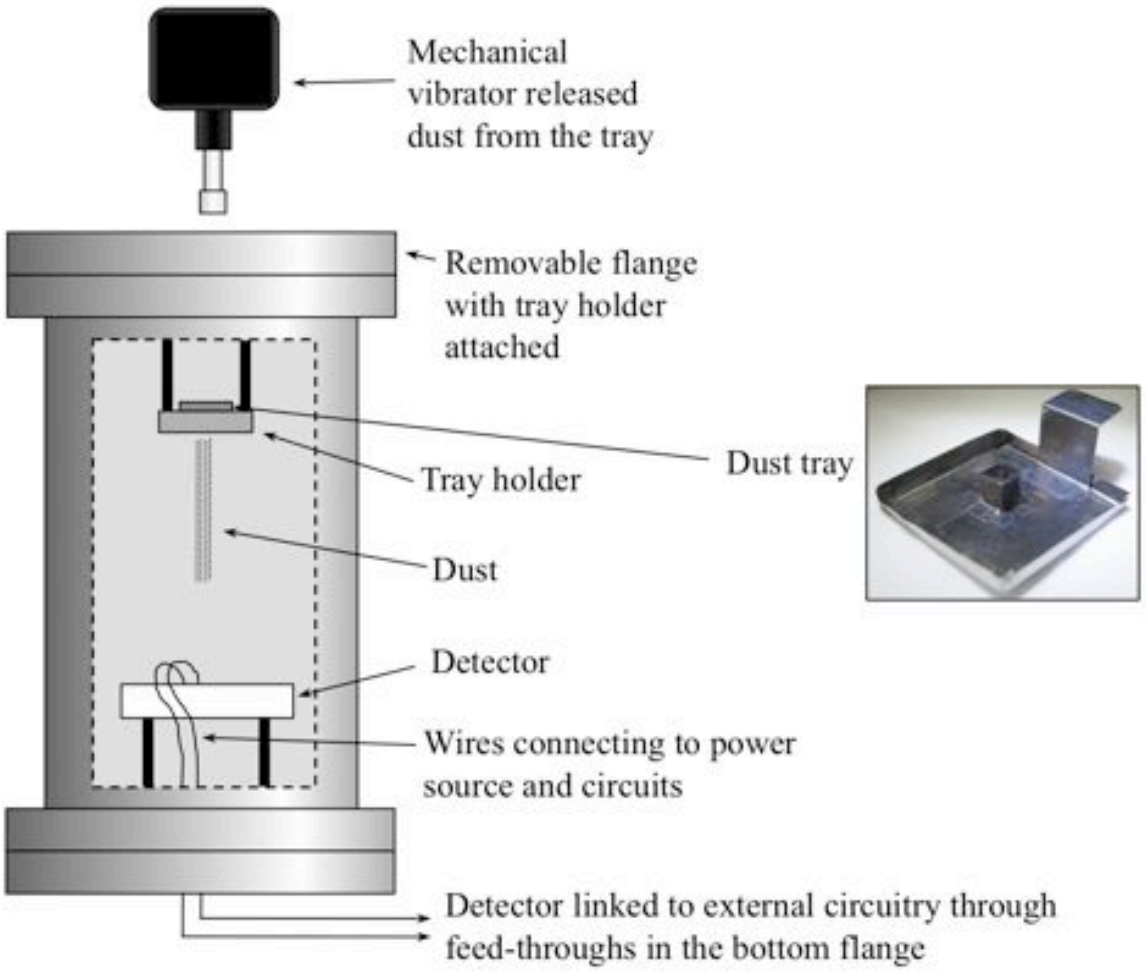

Fig. 7: Laboratory setup.

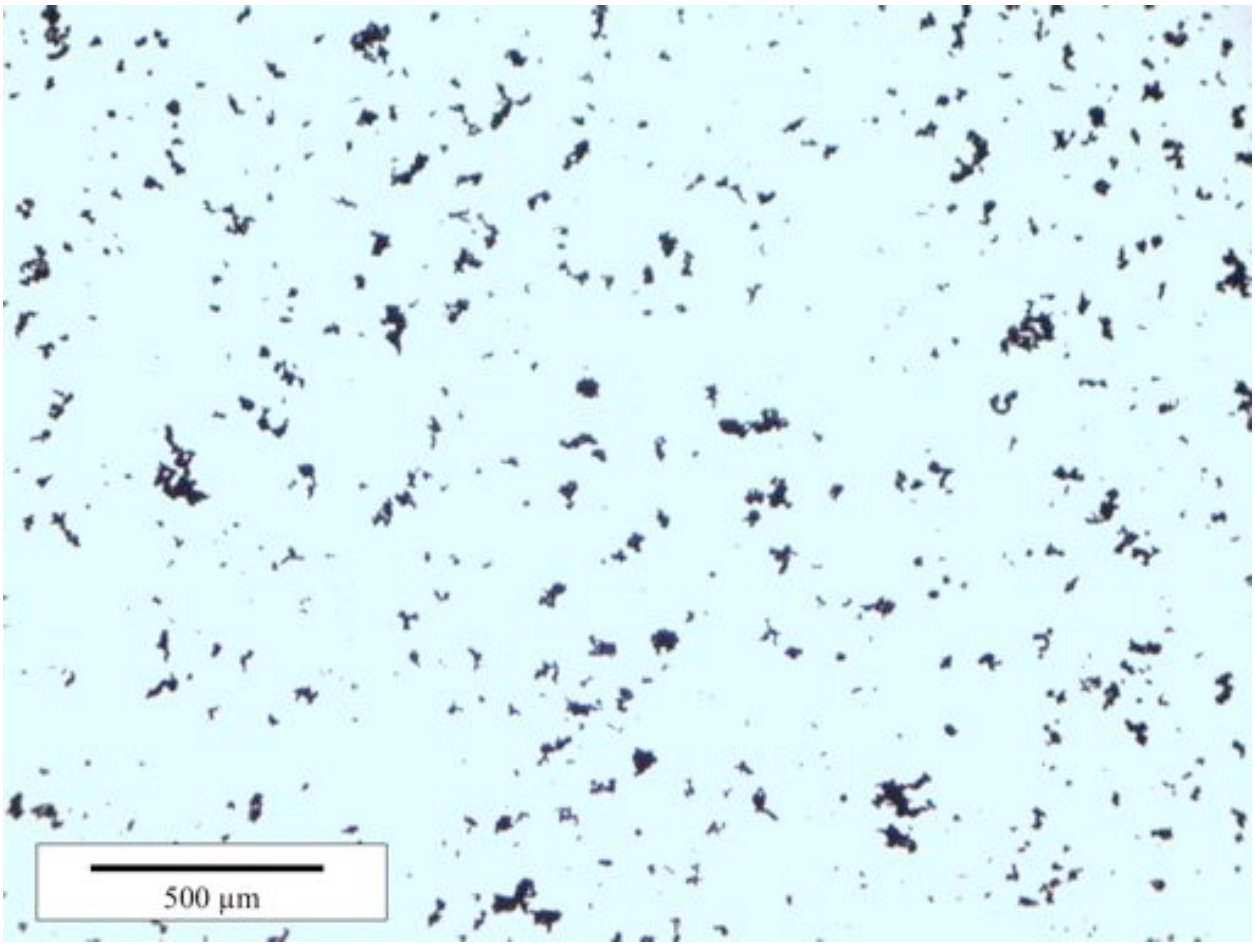

Fig. 8: Microscope image (4x magnification) of tungsten particles used in this experiment. The width of the image is approximately 2.67mm.

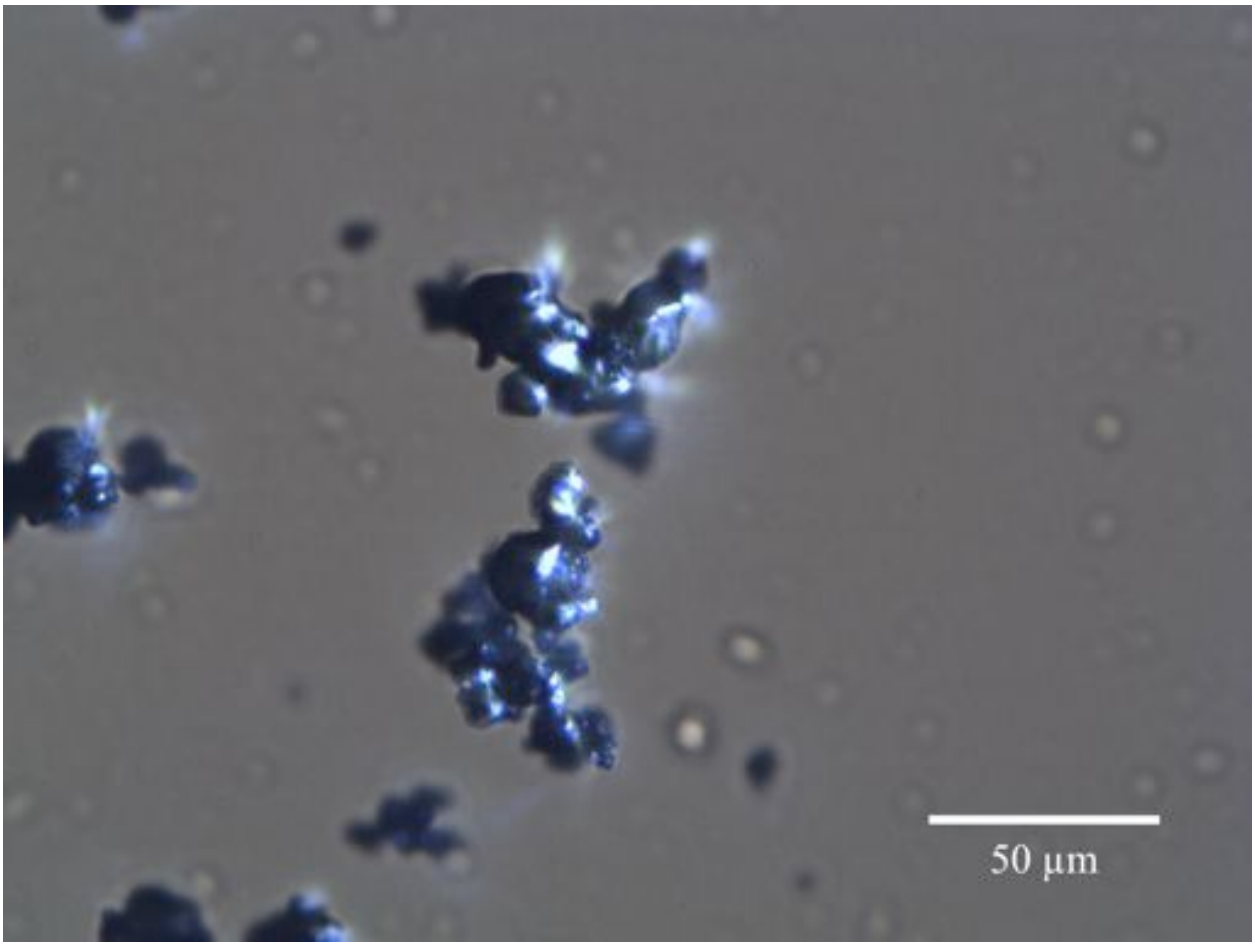

Fig. 9: Microscope image at 40x magnification showing examples of clumping. Image is approximately 270µm wide.

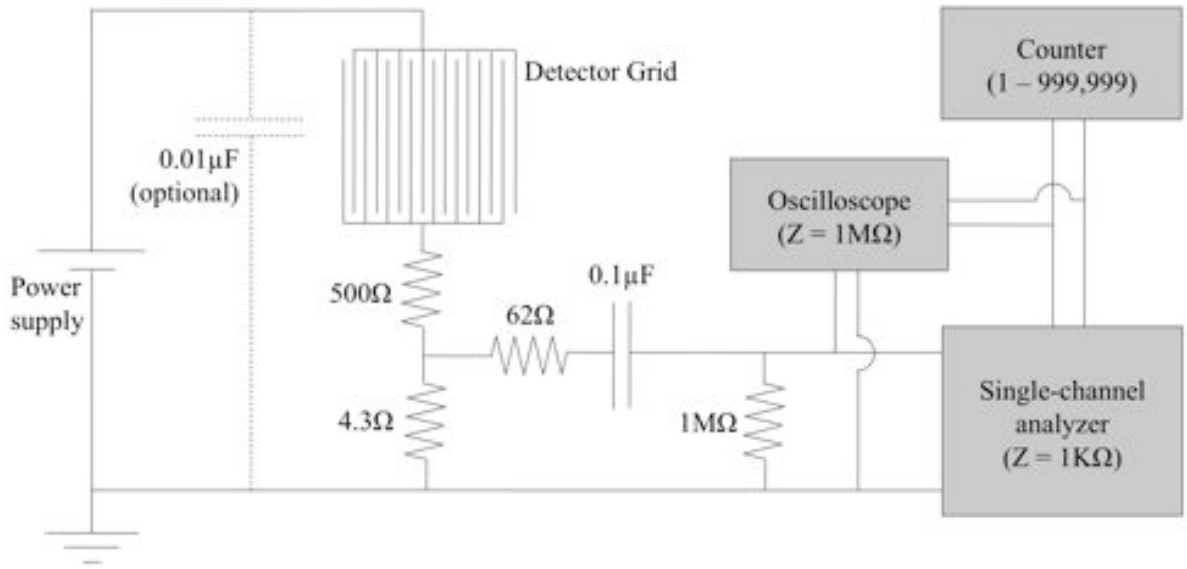

Fig. 10: Schematic of the circuit used for the tests. The 500Ω and 4.3Ω resistors adjust the magnitude of the signal received by the oscilloscope and SCA. The 62Ω resistor was part of a low-pass filter used in previous experiments.

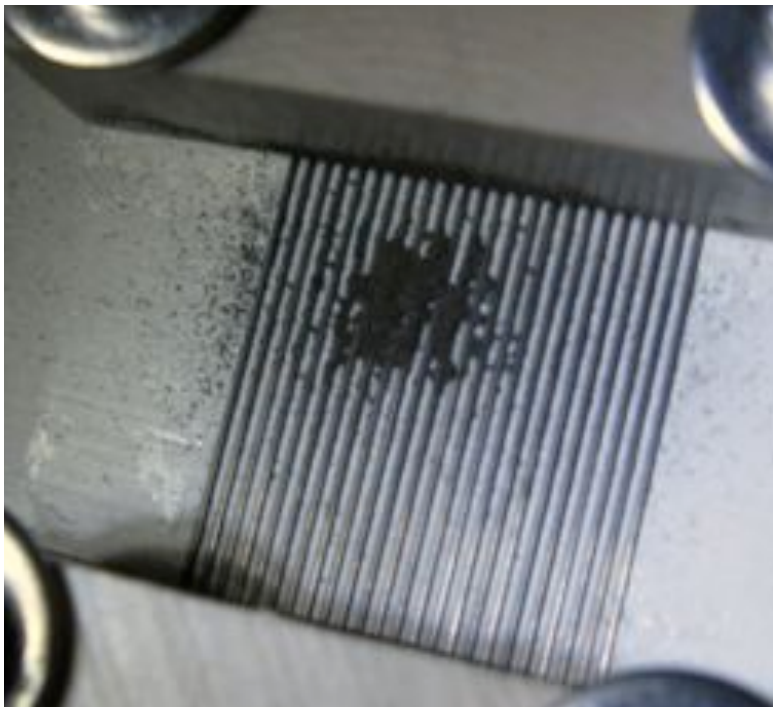

Fig. 11: Rectangular detector after dust deposition while energized to 150V.

Fig. 12: Rectangular detector after dust deposition while energized to 200V.

Fig. 13. Rectangular detector after dust deposition while energized to 250V.

Fig. 14: Rectangular detector after deposition while energized to 300V.

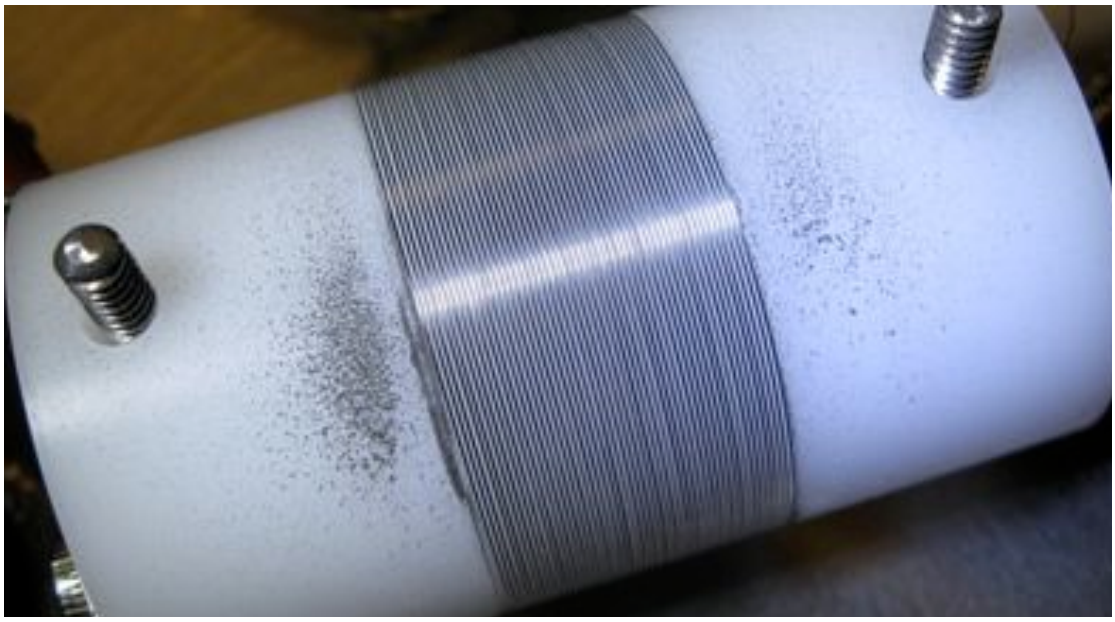

Fig. 15: Cylindrical detector after deposition while energized to 350V.

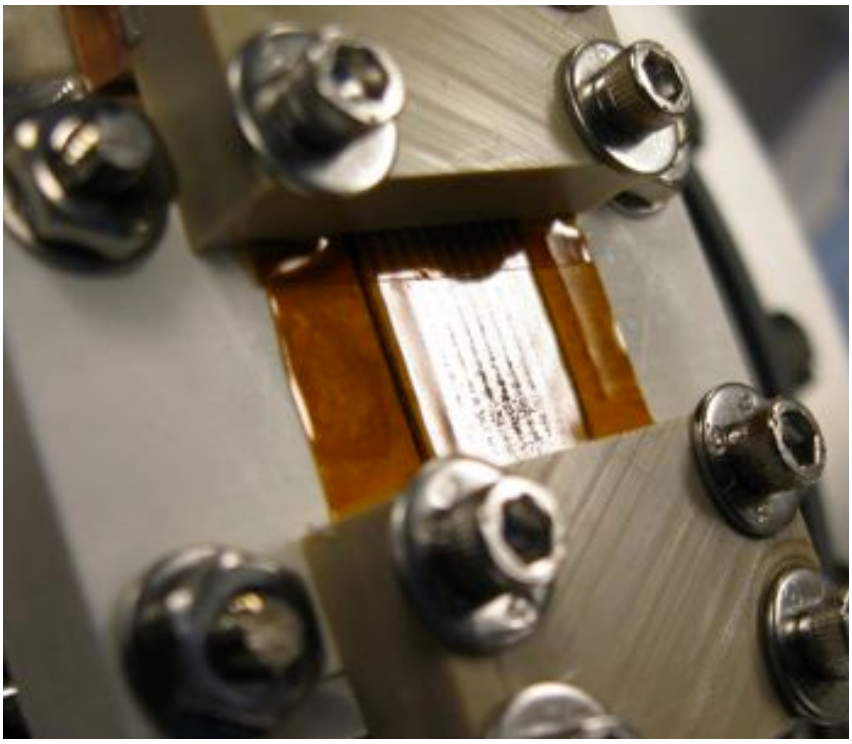

Fig. 16: Dust deposition on a rectangular detector whose wires were covered with insulating tape. Dust has lined up along the wires that were at high voltage. (Note: this particular detector had wire diameters and spacing of 0.50 mm, twice that of the rectangular detector referred to by default in this paper.)

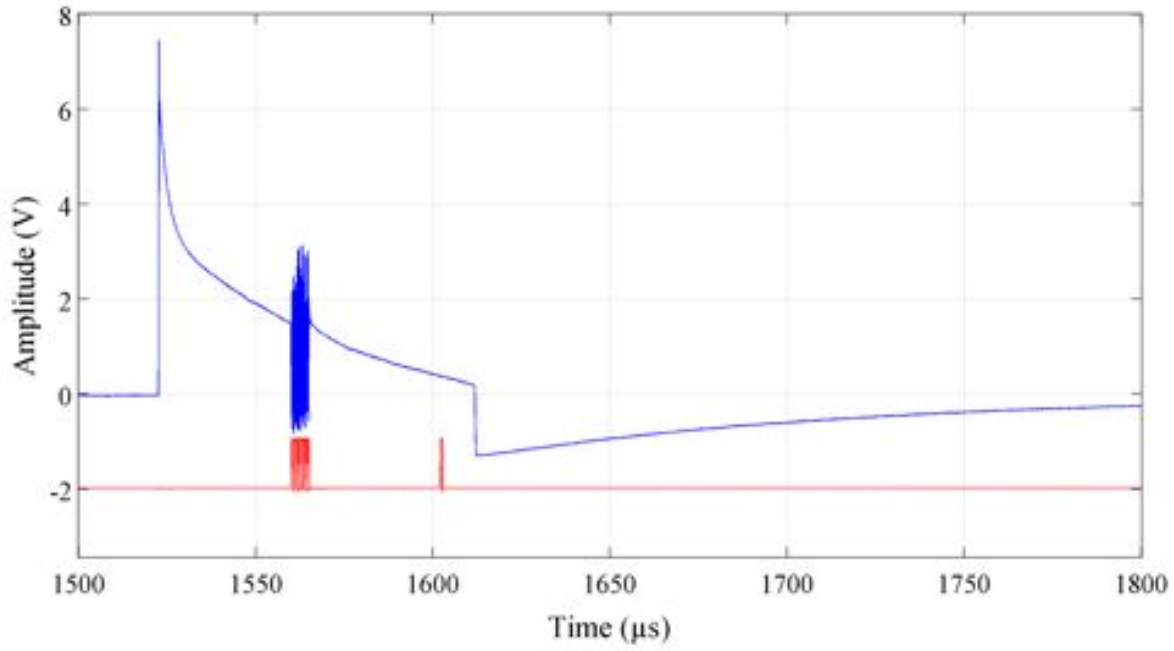

Fig. 17: Signal from the rectangular detector during a short circuit at 800V (top) and the response pulses from the SCA (bottom; offset and scaled for clarity). A 0.01 μF capacitor was in parallel with the power supply. Note that in absence of the rapid oscillations, the signal would have generated only one SCA pulse (the one at ~ 1600 μs). Time is measured relative to the triggering of the oscilloscope.

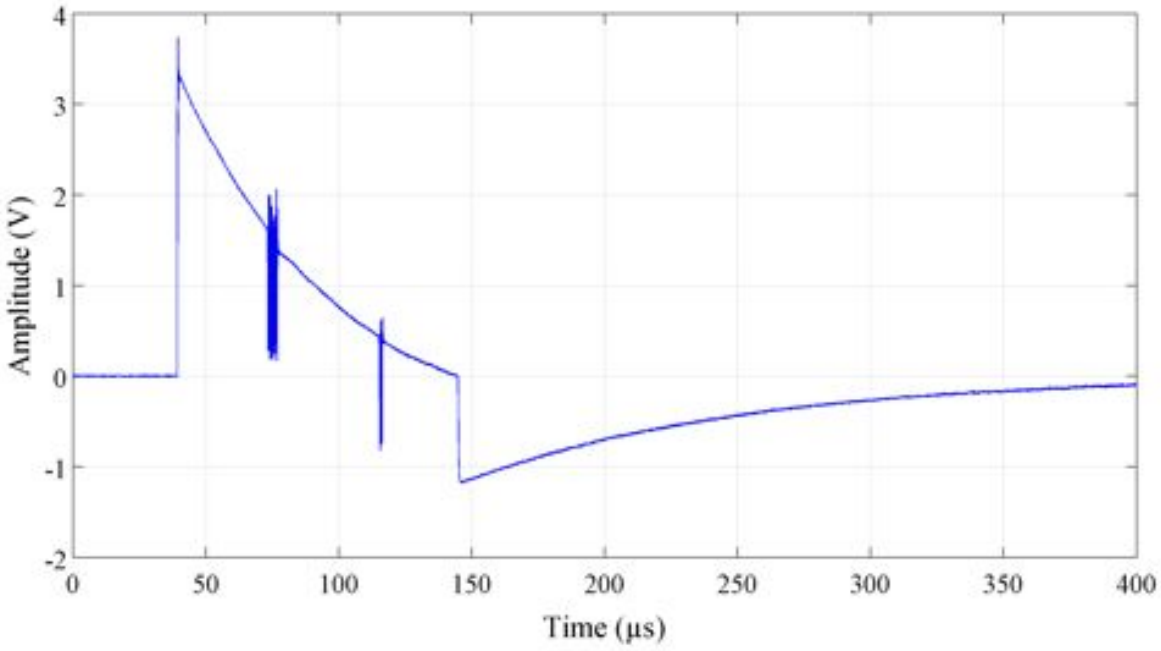

Fig. 18: Typical signal from the rectangular detector biased to 800 V with no capacitance in parallel with the power supply.

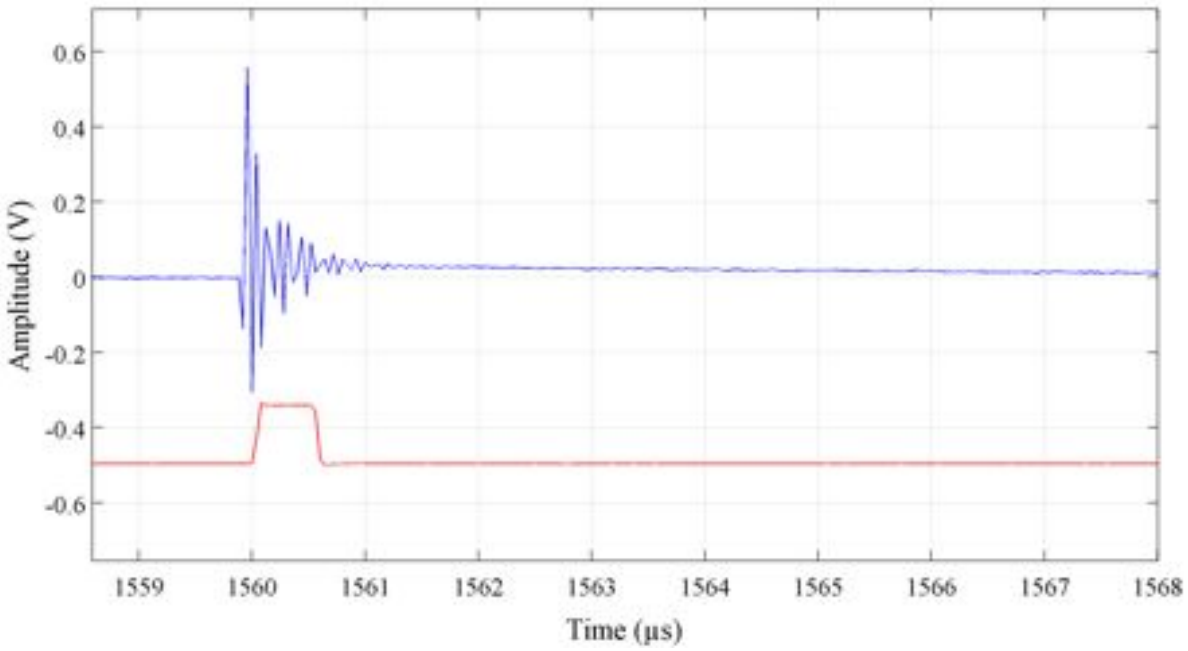

Fig. 19: Signal from cylindrical detector during a short circuit at 350 V (top) and response pulses from the SCA (bottom; offset and scaled for clarity). A 0.01 μF capacitor was in parallel with the power supply. Time is measured relative to the triggering of the oscilloscope.

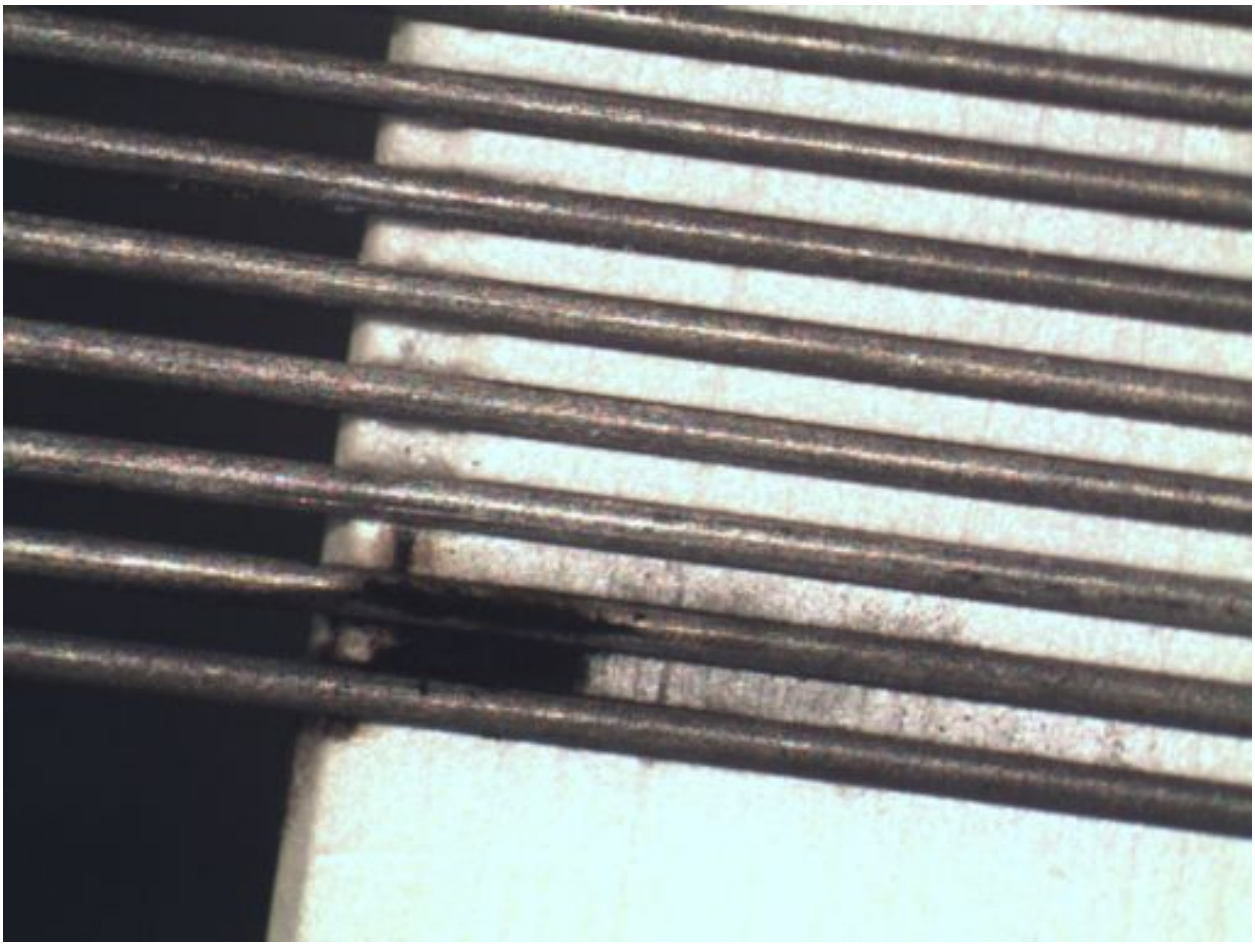

Fig. 20: Example of a conducting stain found on the rectangular detector, underneath a PEEK clamp.

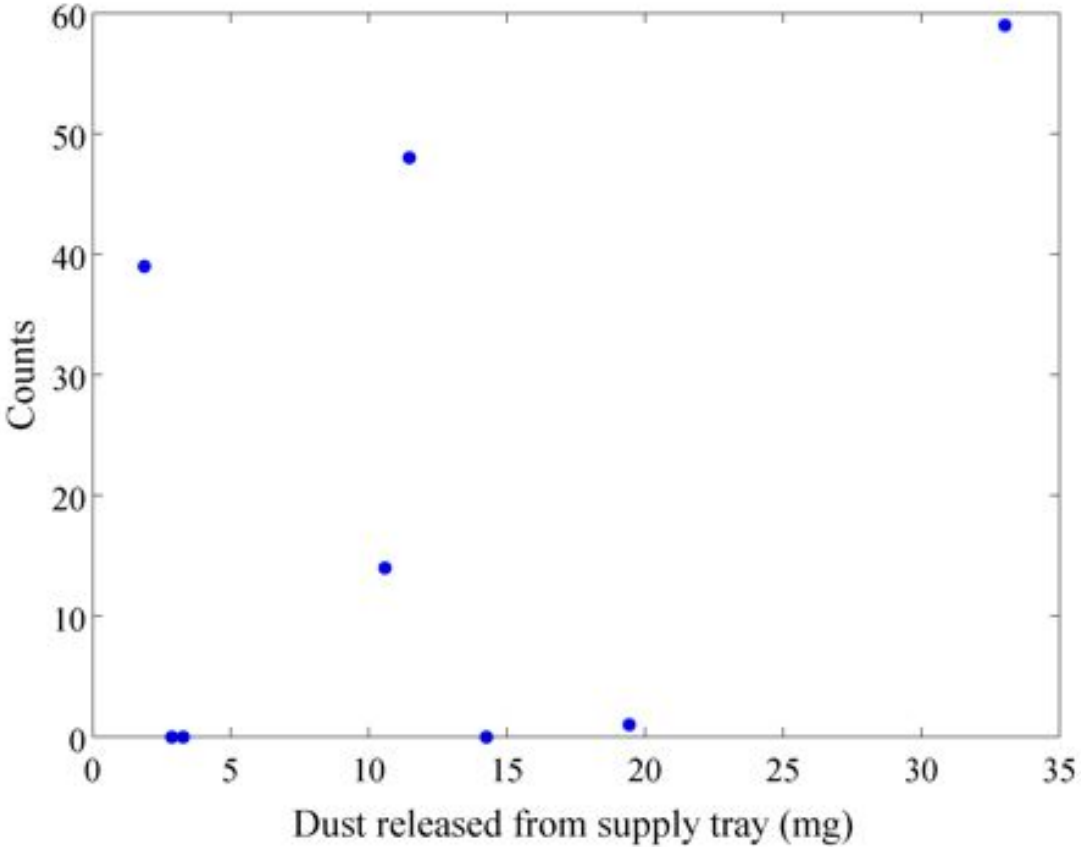

Fig. 21: Scatter plot of counts recorded for given amounts of dust released from the supply tray for the rectangular detector energized to 800V.

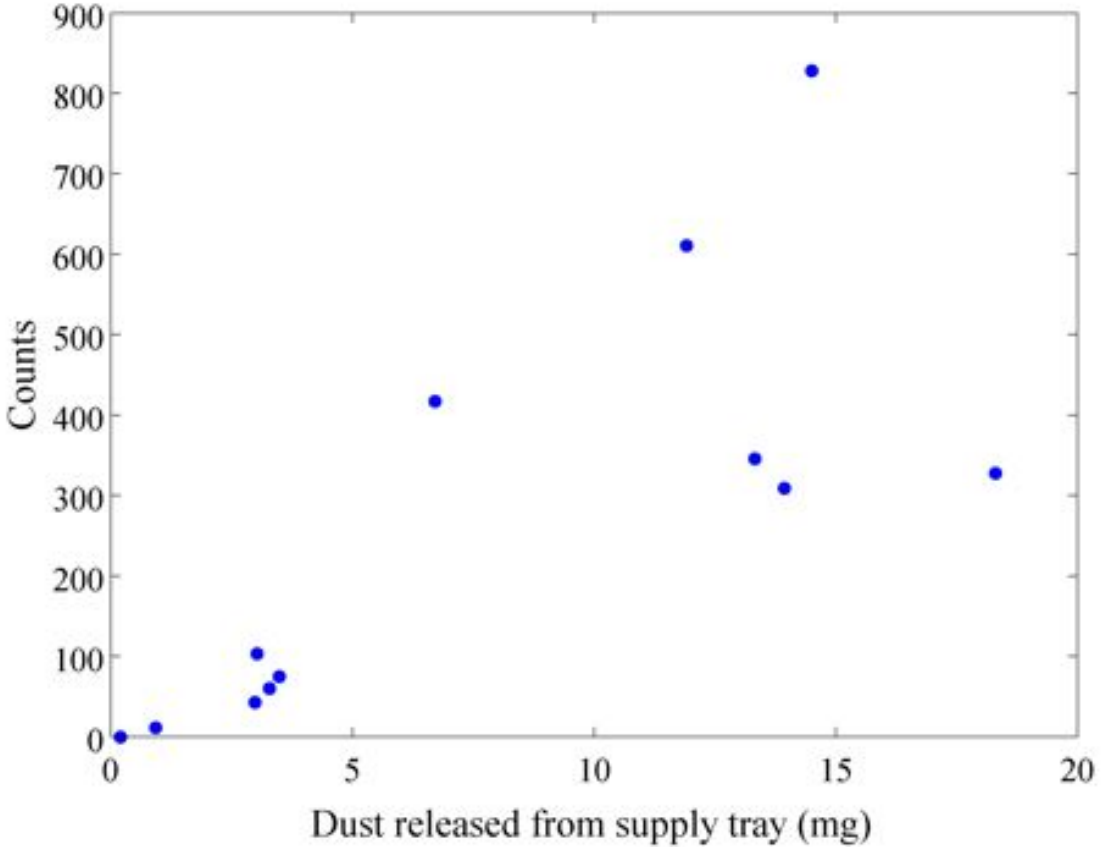

Fig. 22: Scatter plot of counts recorded for mass released from the supply tray for the cylindrical detector energized to 350V.

The Princeton Plasma Physics Laboratory is operated
by Princeton University under contract
with the U.S. Department of Energy.

Information Services
Princeton Plasma Physics Laboratory
P.O. Box 451
Princeton, NJ 08543

Phone: 609-243-2245
Fax: 609-243-2751
e-mail: pppl_info@pppl.gov
Internet Address: http://www.pppl.gov